Mon. Not. R. Astron. Soc. **000**, 1–12 (2014) Printed 10 August 2015 (MN LaTeX style file v2.2)

arXiv:1508.01740v1 [astro-ph.GA] 7 Aug 2015

The Excitation Mechanism of H_2 in Bipolar Planetary Nebulae

R.A. Marquez-Lugo,[1]* M.A. Guerrero,[1] G. Ramos-Larios[2] and L.F. Miranda[1]
[1] *Instituto de Astrofísica de Andalucía IAA, CSIC, Glorieta de la Astronomía s/n, E-18008 Granada, Spain*
[2] *Instituto de Astronomía y Meteorología, CUCEI, Universidad de Guadalajara, Av. Vallarta No. 2602, Col. Arcos Vallarta, 44130 Guadalajara, Jalisco, Mexico*

today

ABSTRACT

We present near-IR *K*-band intermediate-dispersion spatially-resolved spectroscopic observations of a limited sample of bipolar planetary nebulae (PNe). The spectra have been used to determine the excitation mechanism of the H_2 molecule using standard line ratios diagnostics. The H_2 molecule is predominantly shock-excited in bipolar PNe with broad equatorial rings, whereas bipolar PNe with narrow equatorial waists present either UV excitation at their cores (e.g., Hb 12) or shock-excitation at their bipolar lobes (e.g., M 1-92). The shock-excitation among bipolar PNe with ring is found to be correlated with emission in the H_2 1-0 S(1) line brighter than Brγ. We have extended this investigation to other PNe with available near-IR spectroscopic observations. This confirms that bipolar PNe with equatorial rings are in average brighter in H_2 than in Brγ and show dominant shock excitation.

Key words: ISM: jets and outflows – ISM: lines and bands – infrared: ISM.

1 INTRODUCTION

Planetary Nebulae (PNe) represent the short-lived transition from red gianthood to white dwarfdom for low- and intermediate-mass (1-8 $M_\odot$) stars. These stars eject most of their envelopes at the end of the asymptotic giant branch (AGB). The ejecta forms a circumstellar shell which is subsequently ionized by the central star (CSPN) and becomes a PN. While the optical emission from PNe is dominated by emission lines from ionized gas, molecular material may still survive wherever the optical depth to ionizing photons is high, either in high-density clumps or in photo-dissociation regions (PDR, Tielens & Hollenbach 1993).

Near-infrared imaging of the H_2 1-0 S(1) λ2.122 μm emission line has been used to detect molecular material at high spatial resolution and sensitivity. Since the first detection of H_2 emission in NGC 7027 (Treffers et al. 1976), the near-IR H_2 1-0 S(1) line has been detected in over 100 PNe and proto-PNe (Kastner et al. 1996; Hora, Latter, & Deutsch 1999; Guerrero et al. 2000; García-Hernández et al. 2002, and references therein). These observations show that H_2 emission is predominantly detected in the equatorial regions of bipolar PNe (hereafter BPNe), as self- and dust-shielding of UV photons at PDRs in their dense equatorial regions can provide a safe haven for molecules. Although BPNe are the brightest H_2-emitters, the presence of molecular hydrogen is not exclusive to BPNe; sensitive observations have proven that H_2 emission can also be detected in PNe with ellipsoidal or barrel-like morphologies (Marquez-Lugo et al. 2013). The high-spatial resolution of these observations unveil that the H_2 emission from the equatorial ring of BPNe arises from knots and clumps embedded within the ionized material of the ring rather than from a PDR (Manchado et al. 2015). This is also in concordance with the detection of H_2 emission in bipolar lobes of BPNe (e.g., Ramos-Larios et al. 2008), which points at the presence of molecular material in an environment different from a PDR.

Morphologically, the class of BPNe is not homogeneous, with two distinct sub-classes (Manchado et al. 1996): BPNe with a compact core or narrow waist (W-BPNe), and BPNe with a broad ring structure in the waist (R-BPNe). It is unclear whether these two sub-classes of BPNe descend from progenitors in the same mass range, but observed at different evolutionary stages, or they proceed from progenitors of different mass ranges and follow different evolutionary paths (Guerrero et al. 2000). R-BPNe exhibit the brightest H_2 emission and the highest H_2/Brγ flux ratio (Webster et al. 1988; Guerrero et al. 2000). It is tempting to correlate the H_2 emission with the amount of molecular mass and conclude that R-BPNe have larger reservoirs of molecular material and proceed from more massive progenitors. The intensity of the H_2 emission depends strongly on the exci-

---

* E-mail: amarquez@iaa.es

© 2014 RAS

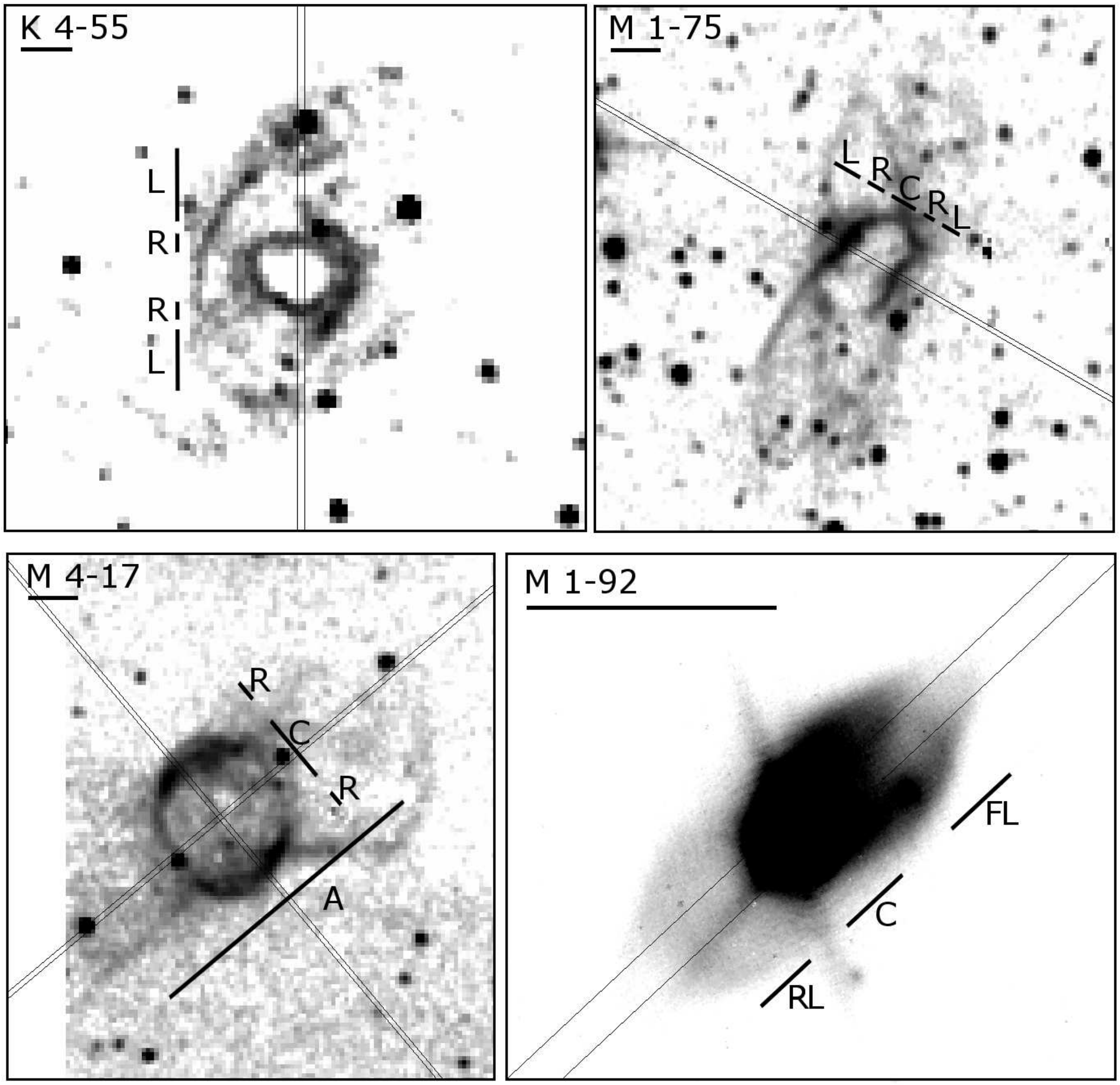

Figure 1. Images in the near-IR H_2 filter of the H_2-bright BPNe in our sample. The slit positions of the near-IR spectroscopic observations and the extent of the spatial apertures used in the extraction of one-dimensional spectra are labeled (see Section 2.1). In all figures, North is up, East left. The horizontal bar below the name of each PN corresponds to $5''$. Note that the linear feature along PA$\sim 10^\circ$ in the image of M 1-92 is an artifact.

tation mechanism, however. In the particular case of BPNe, the typical shock velocities imply higher H_2 emission line intensities than those expected for simple UV-excitation (Burton, Hollenbach, & Tielens 1992). Therefore, imaging in the 2.122 μm H_2 line alone cannot be used to determine the total molecular mass to assess whether the two sub-classes of BPNe are related to different evolutionary stages of the same class of object, or to distinct classes of objects.

To determine the molecular content of the two different sub-classes of BPNe, first we have to establish the excitation conditions of H_2. We have then selected the sample of BPNe listed in Table 1 and obtained moderate-resolution near-infrared *K*-band spectroscopy to diagnose whether the H_2 line ratios are consistent with shock or UV excitation (Black & van Dishoeck 1987). The spectroscopic observations are described in Sect. 2, the spectra and line intensity measurements are presented in Sect. 3, and the investigation of the H_2 excitation mechanism in these PNe is shown in Sect. 4. The results are discussed in Sect. 5 and the main conclusions summarized in Sect. 6.

2 OBSERVATIONS

Near-IR *K*-band spectrophotometric observations of the seven BPNe listed in Table 1 were obtained on July 2-4, 2004 using the 3.5m Telescopio Nazionale Galileo (TNG) and the Near Infrared Camera Spectrometer (NICS) in its spectroscopic mode. A HAWAII 1024×1024 detector was used, resulting in a spectral dispersion of 4.3 Å pixel^{-1} (4.3×10^{-4} μm pixel^{-1}) and a wavelength coverage from 1.925 μm to 2.368 μm. The seeing during the observations varied from $0\farcs7$ up to $1\farcs2$.

For the slit width of $0\farcs75$ used during the observations, the spectral resolution was $\simeq$13Å for a resolution power R $\simeq$1630. The slit position angles (PAs) and total integration times are given in columns 4 and 5 of Table 1, respectively. The spectra were reduced using standard IRAF[1] V2.14.1 routines. The wavelength calibration was obtained using telluric sky lines. The flux calibration was carried out using the standard IR stars of spectral type A–A0 SAO 15832, SAO 48300, and SAO 72320 (Hunt et al. 1998). These same stars were used to correct the nebular spectra from telluric absorptions.

The slits go across the nebular center in all cases along directions of special interest. Figures 1 and 2 show the slit positions on near-IR images of the PNe. Details of the imaging observations are given in Table 2. In the cases of K 4-55, M 1-75, and M 4-17, Figure 1 shows the Calar Alto (CAHA) 2.2 m telescope H_2 images presented by Guerrero et al. (2000), where more details on the observations and data reduction are given. For the other four PNe (Figures 1 and 2), narrow-band near-IR images were obtained at the TNG with NICS in its imaging mode using the Short Field camera in combination with the adaptive optics module. The detector was a 1024×1024 HgCdTe array with pixel size of $0\farcs04$ and field of view of $0\farcm7\times0\farcm7$. Images of Hu 2-1, M 1-92, and IC 4497 were obtained on 2003 September 17-18, while Hb 12 was observed on 2004 September 17. The filter details and exposure times are given in Table 2. The spatial resolution of the images is between $0\farcs4$ and $0\farcs6$. The images were reduced following standard procedures. Figures 1 and 2 show the H_2 images of Hu 2-1, M 1-92, IC 4497, and Hb 12. Their Brγ and K$_{cont}$ images (not shown here) are very similar to the H_2 ones at the angular resolution achieved by these images, showing dominant core emission in all of them and weaker extended emission in the cases of Hb 12 and M 1-92. An attempt to substract the continuum contribution from the H_2 and Brγ line images did not yield satisfactory results given the bright continuum emission at the core of these nebulae.

2.1 Data analysis

The spectra apertures were selected on the basis of the nebular near-IR morphologies (Figures 1 and 2) and spatial profiles of selected spectral emission lines to probe different nebular regions and structures. Additionally, available optical images and kinematical information were used to select these apertures.

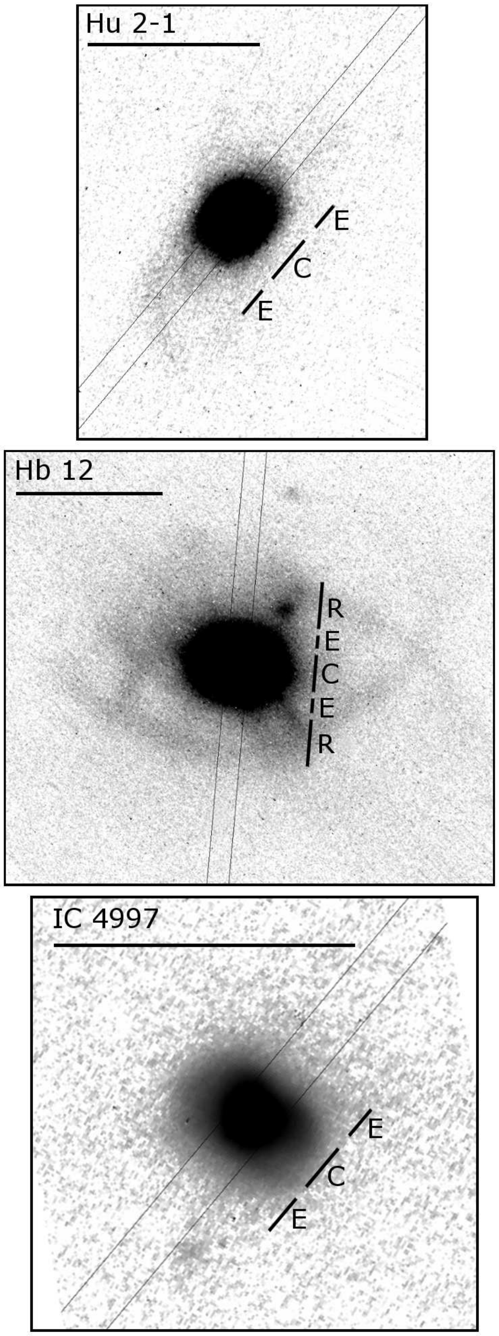

Figure 2. Images in the near-IR H_2 filter of the H_2-weak BPNe in our sample. The slit positions of the near-IR spectroscopic observations and the extent of the spatial apertures used in the extraction of one-dimensional spectra are labeled. In all figures, North is up, East left. The horizontal bar below the name of each PN corresponds to 5″.

The PNe K 4-55, M 1-75, and M 4-17 (Figure 1) are relatively extended sources, with angular sizes many times that of the slit width. They lack a clear identification of their central star. As for K 4-55, the slit PA was selected at 0°, covering the relatively bright central ring (R) and the pole-

---

[1] IRAF, the Image Reduction and Analysis Facility, is distributed by the National Optical Astronomy Observatory, which is operated by the Association of Universities for Research in Astronomy under cooperative agreement with the National Science Foundation.

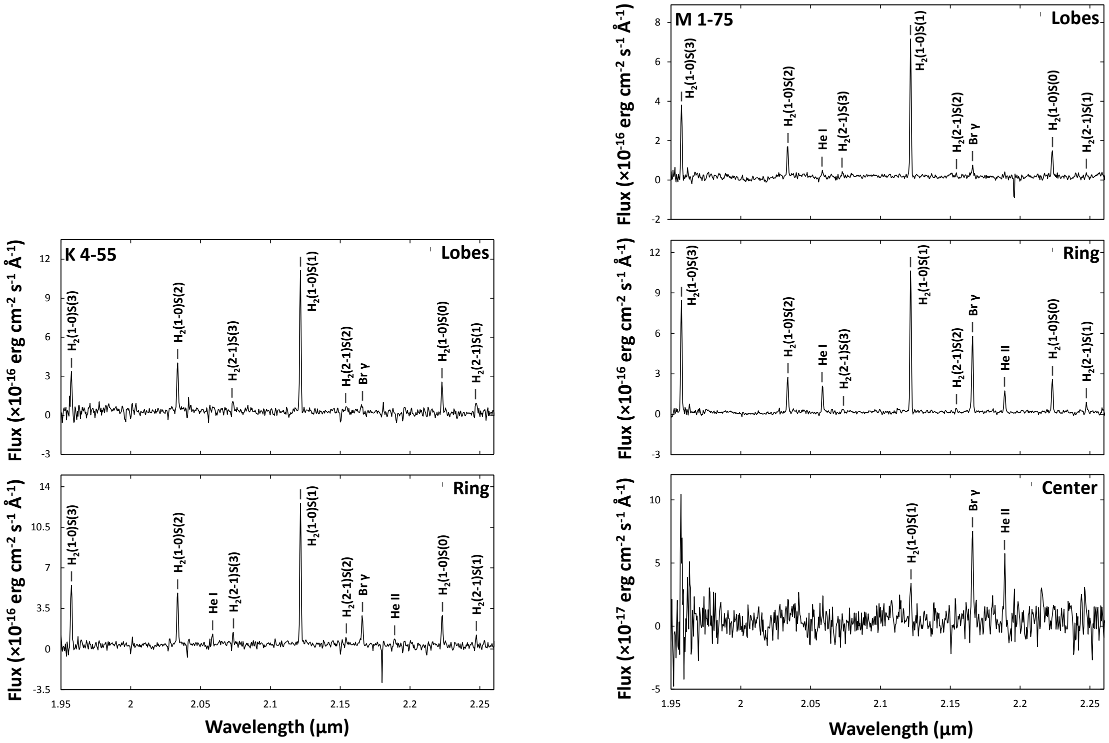

(a) K 4-55

(b) M 1-75

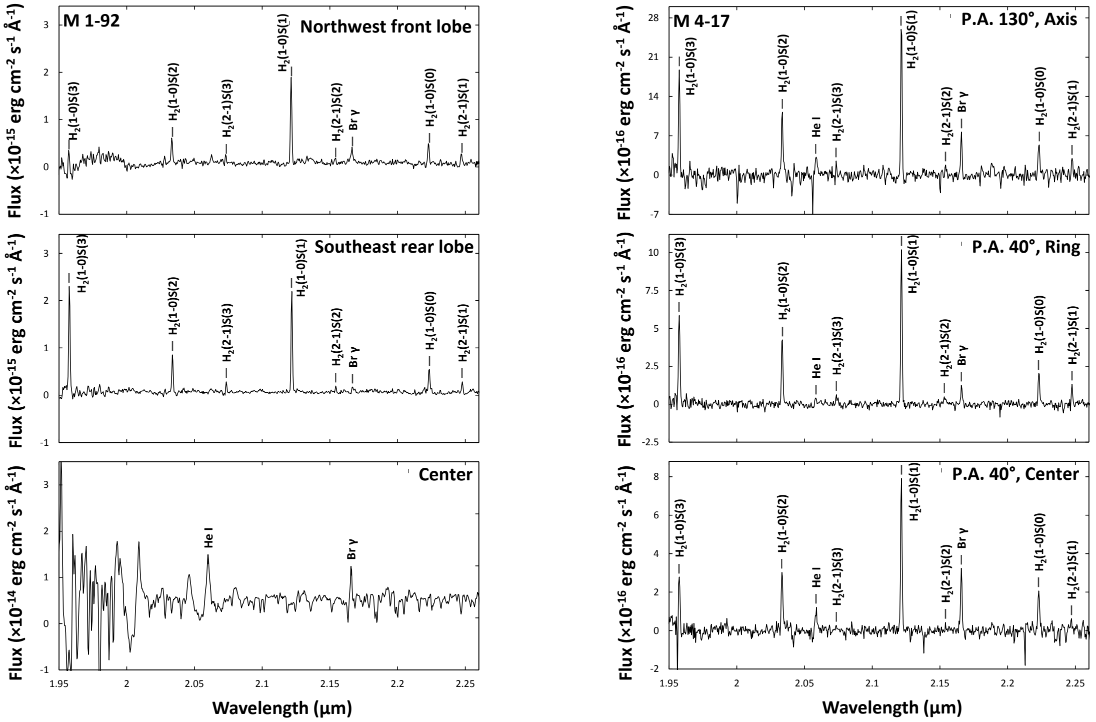

(c) M 1-92

(d) M 4-17

Figure 3. TNG NICS *K*-band spectra of different regions of the H$_2$-bright bipolar PNe K 4-55 (*a*), M 1-75 (*b*), M 1-92 (*c*), and M 4-17 (*d*). The detected lines are labeled on the spectra.

Table 2. Details of the imaging observations.

Source	Telescope	Instrument	Filter	λ_c (μm)	$\Delta\lambda$ (μm)	Exposure time (s)
Hb 12	TNG	NICS	H_2	2.122	0.032	720
Hu 2-1	TNG	NICS	H_2	2.122	0.032	1620
IC 4997	TNG	NICS	H_2	2.122	0.032	1800
K 4-55	2.2m CAHA	MAGIC	H_2	2.122	0.021	100
M 1-75	2.2m CAHA	MAGIC	H_2	2.122	0.021	100
M 1-92	TNG	NICS	H_2	2.122	0.032	600
M 4-17	2.2m CAHA	MAGIC	H_2	2.122	0.021	100

Table 4. Brγ normalized fluxes of H_2-weak BPNe.

Line ID	Wavelength (μm)	IC 4997 P.A. 140°		Hu 2-1 P.A. 320°		Hb 12 P.A.–5°		
		Envel.	Center	Envel.	Center	Ring	Envelope	Core
He I	1.9541	···	···	···	16.2±0.6	···	···	···
H_2 1-0 S(3)	1.9570	···	···	···	···	···	···	11.8±0.3
H_2 1-0 S(2)	2.0334	···	···	···	···	···	10.1±1.6	···
H_2 8-6 S(3)	2.0425	···	1.7±0.1	···	···	···	10.6±1.6	2.3±0.1
He I	2.0580	25.4±1.3	33.8±1.4	68±5	80.1±1.4	103±7	95±5	107.7±0.5
H_2 2-1 S(3)	2.0732	···	···	···	···	···	9.0±1.5	···
He I	2.1124	···	8.6±0.4	7.8±1.7	7.7±0.4	12.3±2.5	···	9.2±0.2
H_2 1-0 S(1)	2.1218	···	0.6±0.1	···	···	14.8±2.8	25.1±2.5	···
Fe III	2.1460	···	···	···	···	···	5.7±1.2	···
H_2 2-1 S(2)	2.1542	···	···	···	···	···	6.0±1.2	···
He II	2.1614	···	4.2±0.2	6.3±1.5	4.9±0.3	···	···	4.1±0.1
Brγ	2.1658	100±4	100±4	100±6	100.0±1.5	100±7	100±5	100.0±0.5
He I	2.1815	···	0.9±0.1	···	···	···	···	1.5±0.1
Kr III	2.1993	···	···	···	2.7±0.3	···	···	···
H_2 3-2 S(3)	2.2014	···	···	···	···	···	7.7±1.4	···
Fe III	2.2184	···	1.4±0.1	···	1.2±0.2	···	17.6±2.1	1.7±0.1
H_2 1-0 S(0)	2.2234	···	···	···	···	14.8±2.7	15.7±2.0	···
H_2 2-1 S(1)	2.2426	···	0.5±0.1	···	···	18.9±3.1	12.1±1.7	···
F(Brγ)^a	2.1658	63	6100	140	2200	100	210	19000

(a) Flux of the Brγ line in units of 10^{-16} erg cm^{-2} s^{-1}.

Table 1. Details of the spectral observations.

Source	α (J2000)	δ (J2000)	P.A. (°)	Exposure time (s)
Hb 12	23 26 14.8	+58 10 55	−5	200
Hu 2-1	18 49 47.6	+20 50 39	320	600
IC 4997	20 20 08.7	+16 43 54	140	600
K 4-55	20 45 10.0	+44 39 16	0	600
M 1-75	20 04 44.1	+31 27 24	60	450
M 1-92	23 26 14.8	+58 10 55	313	120
M 4-17	20 09 01.9	+43 43 44	40	600
			130	600

on bipolar lobes (L) at the position where they intersect (Guerrero, Manchado, & Serra-Ricart 1996). M 1-75 has a quadrupolar morphology (Manchado, Stanghellini, & Guerrero 1996; Santander-García et al. 2010), with two pairs of bipolar lobes aligned along PA 10° and –30°, i.e. their main axis orientations differ by $\sim$40°. In this case, the slit was oriented at PA 60°, along a direction of bright emission in the central ring and relatively bright emission from one of the pairs of bipolar lobes outside the ring. Three apertures were used to extract spectra corresponding to the central region (C), equatorial ring (R), and bipolar lobes (L). Finally, as for M 4-17, the observations were acquired using two slits along perpendicular PAs 40° and 130°. The spectrum from the first slit, along the equatorial direction, allowed us to extract one-dimensional spectra of the central region (C) and equatorial ring (R). The second slit goes along the nebular bipolar axis, where the emission is weaker than along the equatorial direction. In this case, all the emission detected in the slit was added into a single one-dimensional spectrum (A) which is representative of the whole nebula.

In contrast with the sources described above, Hb 12, Hu 2-1, IC 4997, and M 1-92 (Figures 1 and 2) have smaller angular sizes, of the order of the slit width. Among these four sources, Hb 12 shows the most detailed near-IR structure, which can be described as a series of nested equatorial arcs surrounding a dense core in an eye-shaped structure at the center of a more extended hourglass nebula (Hora & Latter 1996; Dinerstein et al. 1988; Welch et al. 1999; Hora et al. 2000; Clark et al. 2014). The slit was oriented along the bipolar axis at PA=−5°, covering the core (C), core envelope

Table 3. Brγ normalized fluxes of H_2-bright BPNe.

Line ID	Wavelength (μm)	K 4-55 P.A. 0°		M 1-75 P.A. 60°			M 4-17 P.A.130°	M 4-17 P.A.40°		M 1-92 P.A.313°		
		Lobes	Ring	Lobes	Ring	Center	All	Ring	Center	F. lobe	R. lobe	Center
H_2 1-0 S(3)	1.9570	400±50	217±18	480±50	140±10	···	196±27	345±31	82±4	49±11	838±34	···
H_2 1-0 S(2)	2.0334	510±50	185±17	211±33	48±6	···	139±14	247±26	91±4	56±4	297±20	···
He I	2.0580	···	39±8	96±22	34±5	···	65±7	32±10	48.2±2.3	···	···	300±4
H_2 2-1 S(3)	2.0732	104±24	33±7	27±12	4.9±1.8	···	21.5±3.1	47±12	14.5±1.2	17.5±2.3	79±11	···
H_2 1-0 S(1)	2.1218	1370±90	452±26	830±70	176±11	47.7±2.8	307±31	530±40	210±9	153±7	723±32	···
H_2 2-1 S(2)	2.1542	110±22	16±5	36±14	6.7±2.1	···	52±5	53±12	17.2±1.3	18.9±2.4	58±9	···
Brγ	2.1658	100±22	100±13	100±23	100±8	100±5	100±10	100±17	100±4	100±6	100±12	100.0±2.0
He II	2.1892	···	28±7	···	30±5	61.9±2.5	···	···	···	···	···	···
H_2 1-0 S(0)	2.2234	310±40	107±13	212±31	45±6	···	98±10	120±18	88±4	44±4	213±17	···
H_2 2-1 S(1)	2.2426	152±29	25±6	67±19	14.3±3.1	···	47±5	61±13	27.2±1.8	30.4±3.1	105±12	···
F(Brγ)^a	2.1658	8.1	33	9.8	74	11	120	25	52	160	36	1300

(a) Flux of the Brγ line in units of 10^{-16} erg cm^{-2} s^{-1}.

(E), and ring (R). The optical structure of Hu 2-1 is complex, with a central equatorial ring containing a small elliptical shell, a pair of bipolar lobes, two pairs of collimated bipolar knots, and outer structures (Miranda et al. 2001). Radio continuum observations of IC 4997 reveal an outer bipolar shell and an inner elliptical one (Miranda & Torrelles 1998). Otherwise, both Hu 2-1 and IC 4997 are rather compact in the near-IR images shown in Figure 2, with relatively bright emission at their central regions and much fainter extended emission. The slit PAs were selected to cover the main nebular axis in the case of Hu 2-1, and the minor nebular axis in the case of IC 4997, but in view of their inconspicuous near-IR morphology, one-dimensional spectra have been extracted for the central regions (C) and extended emission (E). Finally, M 1-92, the Minkowski's Footprint Nebula, has a clear bipolar morphology, with the nebular axis oriented along PA 313° (Trammell & Goodrich 1996; Bujarrabal et al. 1998). The Southeast lobe is fainter than the Northwest one because the inclination of the nebula causes differential extinction by an extended equatorial disk. The slit was placed along the nebular axis, covering the Northwest (front) lobe (FL), the central region (C), and the Southeast (rear) lobe (RL).

3 ONE-DIMENSIONAL SPECTRA

The one-dimensional spectra of the selected regions in our sample of PNe are shown in Figures 3 and 4. The distribution of the different spectra in these two figures is not accidental: PNe in Figure 3 show spectra rich in emission lines of molecular hydrogen, whereas the spectra of PNe in Figure 4 have weak or absent H_2 lines, but bright H I and He I lines. Accordingly, we have split the PNe in our sample into two groups, the H_2-bright PNe K 4-55, M 1-75, M 1-92, and M 4-17, and the H_2-weak PNe Hb 12, Hu 2-1, and IC 4997.

The line identifications and their rest wavelengths, and the normalized line intensities in the selected regions (see Figs. 3 and 4) of the H_2-bright PNe are listed in Table 3, and those of the H_2-weak PNe in Table 4.

Line ratios have not been undereddened since the visual absorption towards these PNe imply A_K <0.15 mag, which result in line relative intensities corrections in the full K-band smaller than 5%. The results in these tables confirm the segregation of the PNe in our sample into two different groups. The H_2-bright PNe in Table 3 have a large number of H_2 emission lines in the near-IR K-band and show H_2 1-0 S(1) to Brγ line ratios much larger than unity. On the contrary, the H_2-weak PNe in Table 4 show a small number of H_2 emission lines, these are generally weak, and the Brγ line is much brighter than the H_2 1-0 S(1) line when the latter is detected.

The spectral properties of the H_2-bright and H_2-weak PNe are described in further detail in the next sections.

3.1 H_2-bright BPNe

The near-IR images of the H_2-bright BPNe K 4-55, M 1-75, and M 4-17 display large, well resolved, and bright ring-like structures and extended bipolar lobes. These are typical R-BPNe. The one-dimensional spectra of these PNe have been extracted from regions corresponding to the outer bipolar

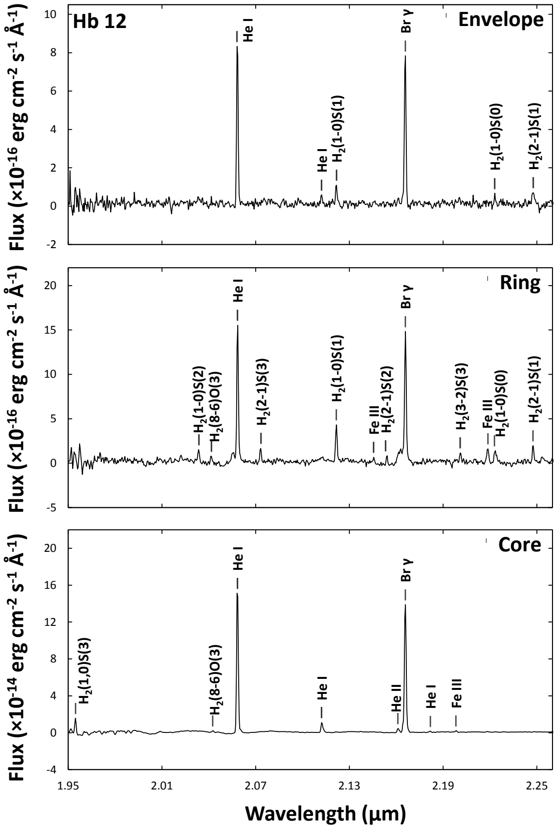

(a) Hb 12

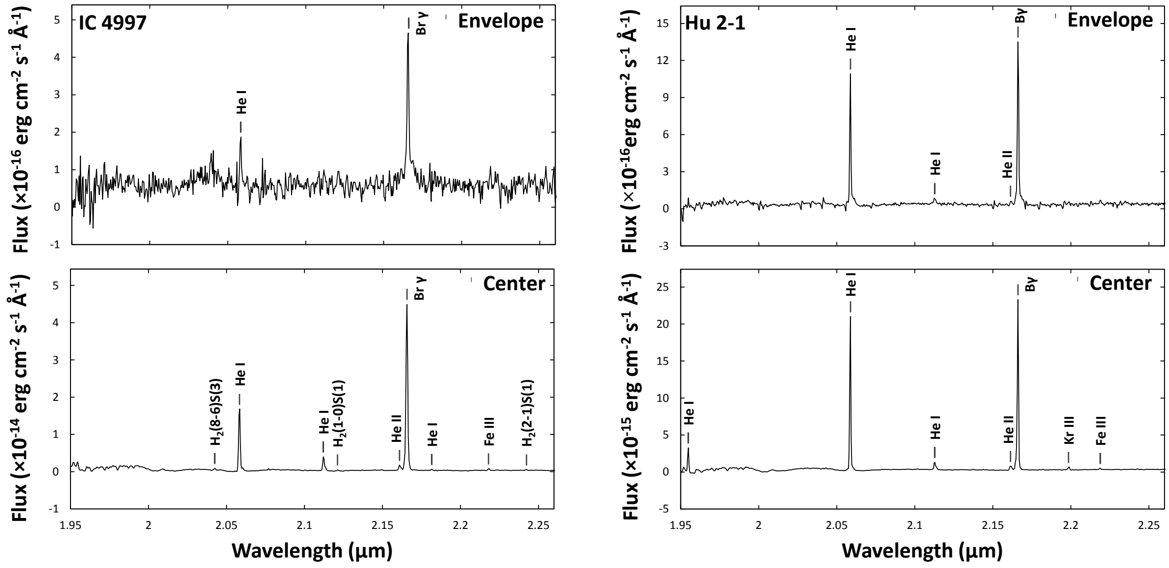

(b) IC 4997

(c) Hu 2-1

Figure 4. TNG NICS *K*-band spectra of different regions of the H_2-weak PNe Hb 12 (*a*), IC 4997 (*b*), and Hu 2-1 (*c*). The detected lines are labeled on the spectra.

lobes, the central ring, and the interior of this ring. As for M 4-17, the emission from the bipolar lobes was found too weak, and it has been merged into one single spectrum for the whole nebula.

On the other hand, M 1-92 has relatively bright bipolar lobes, but the central region is not resolved into a ring, but it is better described as a bright core-like feature, i.e., it is a W-BPN. In this case, the one-dimensional spectra correspond to the bipolar lobes and the core. The spectra of the two bipolar lobes have been considered separately as they show differing surface brightness and line ratios.

The bipolar lobes of these sources are characterized by extreme ratios between the H_2 1-0 S(1) and Brγ emission lines, with values ranging from $\sim$7 (rear lobe of M 1-92) up to $\sim$14 (K 4-55). Other lines from ionized species (He I and He II) are equally faint. Otherwise, several emission lines from other H_2 transitions are quite bright.

The ring-like structures of K 4-55, M 1-75, and M 4-17 still display numerous and bright H_2 emission lines, but their intensity, relative to that of Brγ and He I and He II lines, is lower. As for the innermost region of M 1-92, the H_2 lines are undetected. This is also the case for the central regions of M 1-75, whereas, in the case of M 4-17, H_2 lines are still present, but weak. The projection of the bipolar lobes on the innermost regions of M 4-17 would explain the detection of H_2 emission there.

The above description of the near-IR *K*-band spectra of H_2-bright BPNe suggests a scenario where the innermost regions of these nebulae are dominated by ionized material, whereas molecular material is found (and excited) in ring-like structures and bipolar lobes. Material close to the central star exhibits higher ionization degrees, as implied by the intensity of the He I and even He II emission lines, but molecular material can still shield from the stellar UV radiation in clumps at ring- or torus-like structures or survive in the bipolar lobes where the UV radiation flux has been diluted by the large distance towards the central star.

3.2 H_2-weak BPNe

The PNe in this subsample, Hb 12, Hu 2-1, and IC 4997, are all dominated in the near-IR by the bright emission from an unresolved core (Fig. 1). The outermost emission in these nebulae is much weaker: the eye-shaped feature around the bright core of Hb 12, which has been described as the line where the outer bipolar lobes join (Hora et al. 2000), the weak bipolar lobes of Hu 2-1, and the outer emission from a knot-like feature in IC 4997. Hb 12 can be classified as W-BPN, whereas Hu 2-1 is better described as a R-BPN. The detailed classification of IC 4997 is uncertain.

The near-IR *K*-band spectra from the central regions of these sources are dominated by the Brγ and He I λ2.0580 μm lines. Other He I and even the He II λ2.1614 μm lines are also clearly detected in the spectra of these compact regions. Weak Fe III λ2.1460 μm, Fe III λ2.2184 μm, and Kr III λ2.1993 μm lines are detected in these PNe. The H_2 lines, if present in these spectra, are not that prominent as in the H_2-bright PNe.

The spectra of the outer regions of these nebulae have much lower signal-to-noise ratio than those of their inner regions. Hu 2-1 shows Brγ and He I and He II lines, whereas the spectrum of the outer emission in IC 4997 only displays the Brγ and He I λ2.0580 μm line. The eye-shaped feature of Hb 12 shows the most interesting spectrum, with a number of H_2 and Fe III lines in addition to the Brγ, He I λ2.0580 μm, and He II λ2.1614 μm lines. Similar to the results reported by Hora & Latter (1996) and Hora, Latter, & Deutsch (1999).

To conclude, Hu 2-1 and IC 4997 show very little evidence for the presence of molecular material, whereas Hb 12, although dominated by emission from ionized material, shows some evidences of molecular material in the outer regions.

4 H_2 EXCITATION

The near-IR *K*-band includes a number of emission lines from ro-vibrational transitions of the H_2 molecule. In particular, the emission lines of several transitions from the vibrational levels 2–1 and 1–0 are very prominent in this band. The H_2 1–0 S(1) to 2–1 S(1) and 3–2 S(3) line ratios have been traditionally used to diagnose the excitation mechanism of the H_2 molecules. If shock excitation is dominant, then the 1–0 S(1)/2–1 S(1) and 1–0 S(1)/3–2 S(3) line ratios are expected to be high, 10–20 and 10–100, respectively, although lower values of the 1–0 S(1)/2–1 S(1) line ratio, down to $\sim$4, have also been proposed (Shull & Hollenbach 1978; Smith 1995). Even lower values of the 1–0 S(1)/2–1 S(1) line ratio, down to $\sim$4, can be expected in shocked molecular clouds (Shull & Hollenbach 1978), where physical conditions may be not similar to those found in PNe. For the case of UV excitation, as in photo-dissociation regions, models predict 1–0 S(1)/2–1 S(1) and 1–0 S(1)/3–2 S(3) line ratios of 2–3 and $\sim$8, respectively (Burton, Hollenbach, & Tielens 1990; Hollenbach & Natta 1995). It must be noted, however, that for high densities, above 10^5 cm^{-3}, collisional de-excitation can thermalize the low-energy states of UV excited H_2 molecules, thus producing ratios for these lines close to those expected in cases of pure shock excitation (Hollenbach & Natta 1995).

In our sample, we can recognize two different groups among those that show H_2 emission lines. The H_2-bright PNe in Table 3 exhibit large H_2 1–0 S(1)/2–1 S(1) line ratios, from $\sim$5.0 in M 1-92 to $\sim$18 in the ring of K 4-55. The H_2 3–2 S(3) line at λ2.2104 μm is not detected, implying large H_2 1–0 S(1)/3–2 S(3) line ratios. These large line ratios are indicative of shock excitation as collisional de-excitation can be discarded because the electron densities of these sources are much lower than those required ($>10^5$ cm^{-3}) for this mechanism to be efficient: 500 cm^{-3} for K 4-55 (Guerrero, Manchado, & Serra-Ricart 1996), 1100 cm^{-3} for M 1-75 (Guerrero, Stanghellini, & Manchado 1995), 2300 cm^{-3} for M 1-92 (Solf 1994), 100–1000 cm^{-3} for M 4-17 (Kaler et al. 1996). On the other hand, the same line ratios implied by the data in Table 4 for the H_2-weak PNe are much smaller, with H_2 1–0 S(1)/2–1 S(1) in the range 0.8–2.1 for IC 4997 and Hb 12. The H_2 3–2 S(3) line is only detected in the region enveloping the core of Hb 12, for a 1–0 S(1)/3–2 S(3) line ratio $\sim$3.3. We thus conclude that in all cases of H_2-weak PNe where the H_2 lines are detected, there is clear evidence of UV excitation.

The population of the H_2 molecule energy levels provides an accurate assessment of the excitation conditions of these molecules (e.g. Hora & Latter 1994; Hora, Lat-

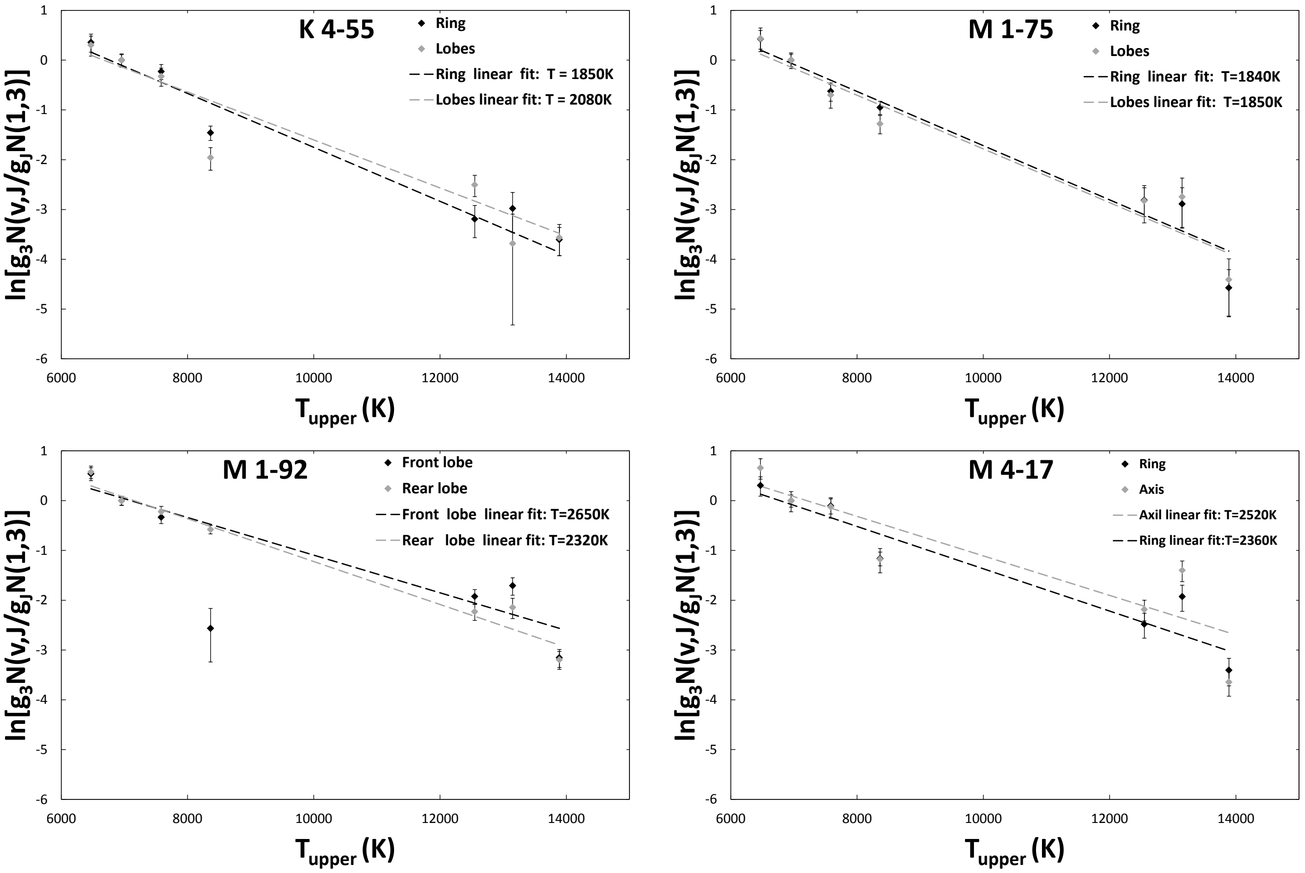

Figure 5. Excitation diagrams for the H_2 lines in the bipolar PNe K 4-55 (top-left), M 1-75 (top-right), M 1-92 (bottom-left), and M 4-17 (bottom-right). Data derived for different regions are plotted with different grey intensities. The linear fits to the different data sets, implying the temperature for thermal excitation, are labeled.

ter, & Deutsch 1999). In the case of pure shock or collisional excitation, a single-temperature Boltzmann distribution describes the population of the energy levels of the H_2 molecule. Then, the value of the vibrational excitation temperature, $T_{ex}(\nu)$, is coincident with the rotational excitation temperature, T_{ex}(J). In the case of UV excitation, the population of the energy levels departs from a Boltzmann distribution and the vibrational and rotational excitation temperatures differ, $T_{ex}(\nu) \neq T_{ex}$(J).

To assess whether excitation is purely collisional or due to UV fluorescence, the H_2 line ratios from the same rovibrational ground levels have been used to derive the column densities relative to the ν= 1 and J=3 state plotted in Figure 5. The data points in these plots can be fitted by a single line, implying that the population of the energy levels follows a Boltzmann distribution and thus that excitation is mostly collisional. A reduced χ^2 fit to these data points indeed confirms that a single line adequately decribes their distribution, with reduced χ^2 values between 0.8 and 1.8. The excitation temperature can be inferred from the slope of the line fitted to the data points: T_{ex}=1850–2080 K for K 4-55, T_{ex}=1840–1580 K for M 1-75, T_{ex}=2320–2650 K for M 1-92, and T_{ex}=2360–2520 K for M 4-17.

As for Hb 12, the H_2 line ratios are consistent with those presented by Hora & Latter (1996) and Luhman & Rieke (1996) who concluded that the excitation mechanism of the H_2 molecules in Hb 12 is pure fluorescent. The available line ratios have been used to derive the column densities relative to the ν= 1 and J=3 state plotted in Figure 6. In this case, the reduced χ^2 for a single linear fit is $\simeq$10, which indicates that the population distribution is not thermal. Different linear fits describe much more accurately the data points from different vibrational levels (reduced χ^2 $\simeq$1.3), thus implying fluorescence excitation. The excitation temperature, $\simeq$990 K, is consistent with that of 1395±450 K reported by Hora & Latter (1996).

Finally, for IC 4997, insufficient emission lines were detected for an analysis of temperature, whereas no H_2 is detected for Hu 1-2.

5 DISCUSSION

A significant fraction of PNe display H_2 emission lines. Most of them have bipolar morphologies, leading Kastner et al. (1994) to state the so-called Gatley's rule, for which the detection of the 2.1218 μm S(1) H_2 line was considered to be conclusive proof of the bipolar nature of a PN. As more sensitive observations are been carried out, many exceptions to this rule have been reported. Large, very evolved PNe of different morphological groups have been found to display emission in H_2 lines (Marquez-Lugo et al. 2013). There is not

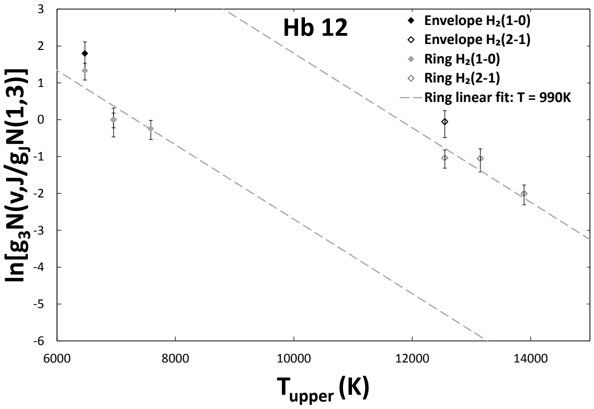

Figure 6. Excitation diagrams for the H_2 lines in the bipolar PNe Hb 12. Data derived for different regions are plotted with different symbols and grey intensities.

a tight correlation between occurrence of H_2 emission and bipolar morphology in fluorescence-excited sources (García-Hernández et al. 2002). The general consensus nowadays is that emission of H_2 lines is not exclusive of PNe with bipolar morphology, although they tend to be brighter in H_2 than other PNe (Marquez-Lugo et al. 2013).

In this work we have presented near-IR *K*-band intermediate-resolution spectroscopic observations of a sample of bipolar and/or elongated PNe. These observations detect H_2 emission lines in Hb 12, K 4-55, M 1-75, M 1-92, and M 4-17. Very weak H_2 emission is also detected in IC 4997. Despite its bipolar morphology, no H_2 emission is detected in Hu 2-1. The high detection rate is not surprising, giving the selection criteria, and it certainly emphazises the higher H_2 brightness of bipolar PNe.

Among our sample, there is a clear correlation between detailed bipolar morphology and relative strength of the H_2 emission: R-BPNe, with well developed equatorial rings and large bipolar lobes tend to exhibit larger H_2 to Brγ line ratios than W-BPNe with narrow waists at their equatorial regions, with the possible exception of Hu 2-1, although we note that its equatorial ring has not developed as those of M 1-75 and M 4-17. This may suggest not only that equatorial rings offer a shelter for H_2 molecules, but that shock excitation, which is a much more efficient excitation mechanism than UV fluorescence and thus produces higher levels of emission in the H_2 lines, is the dominant excitation mechanism in these objects. Indeed, our spectroscopic observations confirm that shock-excitation is prevalent among R-BPNe.

This trend is investigated into more detail in Figure 7, where the H_2 1-0 S(1)/H_2 2-1 S(1) and H_2 1-0 S(1)/Brγ line ratios are plotted for a sample of objects available in the literature (this paper; Hora, Latter, & Deutsch 1999; Lumsden, Puxley, & Hoare 2001; García-Hernández et al. 2002; Davis et al. 2003; Likkel et al. 2006). The distribution of W-BPNe or R-BPNe in this plot confirms the previous trend: R-BPNe outnumber W-BPNe by two to one (12 R-BPNe for 7 W-BPNe) for sources brighter in H_2 than in Brγ, but this ratio reverses for Brγ-brighter sources (6 R-BPNe for 13 W-BPNe for sources with H_2/Brγ <0.5). We also see here trends previously reported on the effects of nebular evolution on the excitation mechanism (and thus in the level) of H_2 emission. In proto-PNe (e.g., CRL 2688) and very evolved bipolar PNe (e.g., M 1-75), where the available flux of ionizing photons is small, the main excitation mechanism of the H_2 molecule would be shocks, whereas in intermediate evolutionary stages, fluorescence might dominate (Davis et al. 2003).

The plot in Figure 7-*left* reveals a loose positive correlation between the H_2 1-0 S(1)/H_2 2-1 S(1) and H_2 1-0 S(1)/Brγ line ratios. When the dominant excitation mechanism is taken into account (Figure 7-*right*), this plot shows that H_2-brighter sources present dominant shock excitation, whereas sources dominated by UV excitation typically have Brγ emission brighter than H_2 1-0 S(1). This confirms shock excitation being more efficient than UV excitation, and thus producing brighter H_2 emissions. We also note that, whereas the sample of H_2-brighter sources are mostly shock excited, there is a non-negligible sub-sample of Brγ-brighter sources that present also shock excitation. As a result, the trend between the H_2 1-0 S(1)/H_2 2-1 S(1) and H_2 1-0 S(1)/Brγ line ratios, which is rather sharp for the H_2-brighter soures, becomes less evident for the Brγ-brighter sources.

The horizontal lines in the plot mark the values of the H_2 1-0 S(1)/H_2 2-1 S(1) ratio typically assumed as lower limit for shock excitation (>10) or upper limit for UV excitation (<3). Within the line ratio uncertainties, the excitation of the different sources in this plot generally follow these rules.

6 CONCLUSIONS

We have presented near-IR *K*-band intermediate-dispersion spatially-resolved spectroscopic observations of a limited sample of bipolar PNe. The spectra have been used to determine the excitation mechanism of the H_2 molecule using standard line ratios diagnostics. Indeed, our spectroscopic observations confirm that shock-excitation is found to be prevalent among R-BPNe with broad equatorial rings, whereas W-BPNe with narrow equatorial waists present either UV excitation at their cores or shock-excitation at their bipolar lobes. The different excitation mechanisms (UV or shock) of the H_2 molecules seem to imply different levels of the H_2 emission with respect to that of Brγ, with larger H_2 1-0 S(1)/Brγ line ratios for shock-excited BPNe, i.e., mostly R-BPNe.

We have investigated possible correlations between different near-IR line ratios, H_2 excitation, and detailed bipolar morphology among PNe with available information in the literature. This study confirms that R-BPNe are in average brighter in H_2 and show dominant shock excitation. We propose the H_2 1-0 S(1)/Brγ line ratio as a preliminary criterion for the excitation mechanism of the H_2 molecules in BPNe, especially in evolved BPNe with a broad equatorial ring, where a high line ratio is very likely the result of shock-excitation.

ACKNOWLEDGMENTS

M.A.G. and R.A.M.-L. are supported by the Spanish MICINN (Ministerio de Ciencia e Innovación) grant AYA

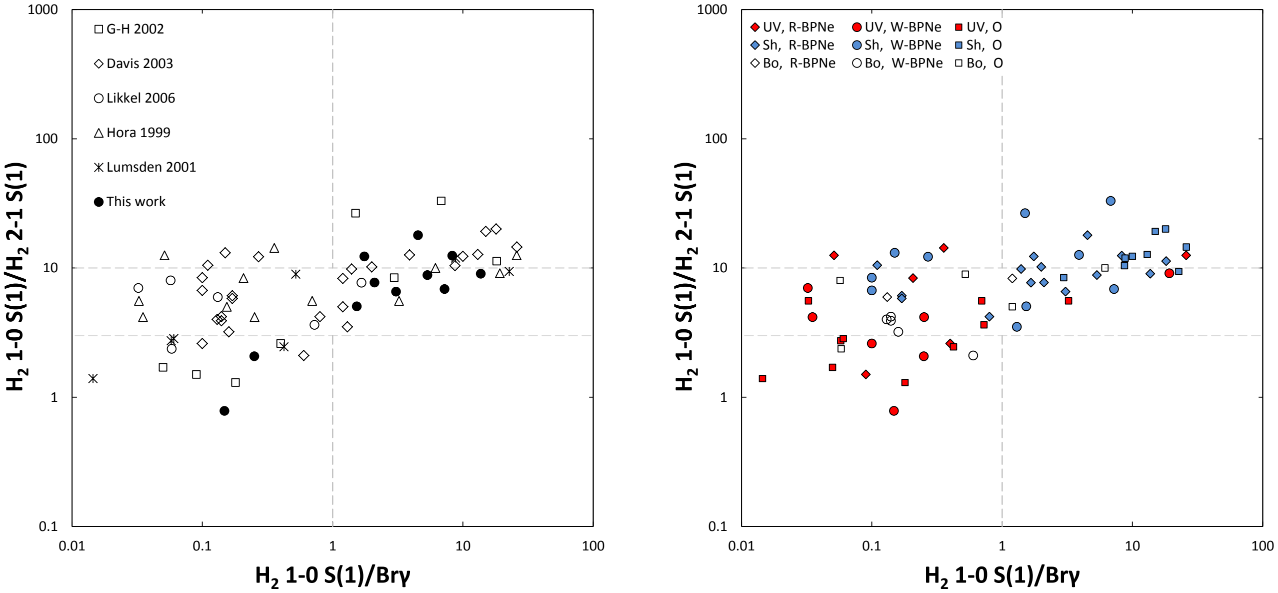

Figure 7. Distribution of PNe in the H_2 1-0 S(1)/H_2 2-1 S(1) versus H_2 1-0 S(1)/Brγ line ratios diagram. *(left)* The sample of PNe with available measurements of these line ratios according to the original reference. *(right)* Same as above, but marking the excitation mechanism and detailed bipolar morphology as waist (W-BPNe) or ring (R-BPNe). Sources with unclear, unknown, or other morphological types are also marked. Sources reported to have a mixture of shock and UV excitation are also singled out. For comparison, the horizontal lines mark the limits for UV-excited (<3) and shock-excited (>10) H_2 typically assumed in the literature. The vertical line at H_2 1-0 S(1)/Brγ unity separates Brγ-bright sources (to the left) from H_2-bright sources (to the right).

2011-29754-C03-02 co-funded with FEDER funds. R.A.M.-L. also acknowledges support by Mexican CONACYT (Consejo Nacional de Ciencia y Tecnología) grant No. 207706. GR-L acknowledges support from CONACYT (grant 177864), CGCI, PROMEP and SEP (Mexico). LFM is supported by the Spanish MICINN grant AYA 2011-30228-C3-01 and MINECO grant AYA 2014-57369-C3-3-P, both co-funded by FEDER funds. Based on observations made with the Italian Telescopio Nazionale Galileo (TNG) operated at the Observatorio del Roque de los Muchachos, La Palma, Spain, by the Fundación Galileo Galilei of the INAF (Istituto Nazionale di Astrofisica). Based on observations collected at the Centro Astronómico Hispano Alemán (CAHA) at Calar Alto, operated jointly by the Max-Planck Institut für Astronomie and the Instituto de Astrofísica de Andalucía (IAA-CSIC).

REFERENCES

Black J. H., van Dishoeck E. F., 1987, ApJ, 322, 412

Bujarrabal V., Alcolea J., Sahai R., Zamorano J., Zijlstra A. A., 1998, A&A, 331, 361

Burton M. G., Hollenbach D. J., Tielens A. G. G. M., 1990, ApJ, 365, 620

Burton M. G., Hollenbach D. J., Tielens A. G. G., 1992, ApJ, 399, 563

Clark D. M., López J. A., Edwards M. L., Winge C., 2014, AJ, 148, 98

Davis C. J., Smith M. D., Stern L., Kerr T. H., Chiar J. E., 2003, MNRAS, 344, 262

Dinerstein H. L., Lester D. F., Carr J. S., Harvey P. M., 1988, ApJ, 327, L27

García-Hernández D. A., Manchado A., García-Lario P., Domínguez-Tagle C., Conway G. M., Prada F., 2002, A&A, 387, 955

Guerrero M. A., Manchado A., Serra-Ricart M., 1996, ApJ, 456, 651

Guerrero M. A., Stanghellini L., Manchado A., 1995, ApJ, 444, L49

Guerrero M. A., Villaver E., Manchado A., Garcia-Lario P., Prada F., 2000, ApJS, 127, 125

Hollenbach D., Natta A., 1995, ApJ, 455, 133

Hora J. L., Latter W. B., 1994, ApJ, 437, 281

Hora J. L., Latter W. B., 1996, ApJ, 461, 288

Hora J. L., Latter W. B., Deutsch L. K., 1999, ApJS, 124, 195

Hora J. L., Latter W. B., Dayal A., Bieging J., Kelly D. M., Tielens A. G. G. M., Trammell S. R., 2000, in Kastner J.H., Soker N. and Rappaport S., eds, ASP Conf. Ser. Vol. 199, Asymmetrical Planetary Nebulae II: From Origins to Microstructures. Astron. Soc. Pac. San Francisco, p. 267

Hunt L. K., Mannucci F., Testi L., Migliorini S., Stanga R. M., Baffa C., Lisi F., Vanzi L., 1998, AJ, 115, 2594

Kaler J. B., Kwitter K. B., Shaw R. A., Browning L., 1996, PASP, 108, 980

Kastner J. H., Gatley I., Merrill K. M., Probst R., Weintraub D., 1994, ApJ, 421, 600

Kastner J. H., Weintraub D. A., Gatley I., Merrill K. M., Probst R. G., 1996, ApJ, 462, 777

Likkel L., Dinerstein H. L., Lester D. F., Kindt A., Bartig

K., 2006, AJ, 131, 1515
Luhman K. L., Rieke G. H., 1996, ApJ, 461, 298
Lumsden S. L., Puxley P. J., Hoare M. G., 2001, MNRAS, 328, 419
Manchado A., Guerrero M. A., Stanghellini L., Serra-Ricart M., 1996, The IAC morphological catalog of northern Galactic planetary nebulae. Instituto de Astrofísica de Canarias (IAC), La Laguna, Spain
Manchado A., Stanghellini L., Guerrero M. A., 1996, ApJ, 466, L95
Manchado A., Stanghellini L., Villaver E., García-Segura G., Shaw R. A., García-Hernández D. A., 2015, arXiv, arXiv:1506.03712
Marquez-Lugo R. A., Ramos-Larios G., Guerrero M. A., Vázquez R., 2013, MNRAS, 429, 973
Miranda L. F., Torrelles J. M., 1998, ApJ, 496, 274
Miranda L. F., Torrelles J. M., Guerrero M. A., Vázquez R., Gómez Y., 2001, MNRAS, 321, 487
Ramos-Larios G., Guerrero M. A., Miranda L. F., 2008, AJ, 135, 1441
Santander-García M., et al., 2010, A&A, 519, AA54
Shull J. M., Hollenbach D. J., 1978, ApJ, 220, 525
Smith M. D., 1995, A&A, 296, 789
Solf J., 1994, A&A, 282, 567
Tielens A. G. G. M., Hollenbach D. J., 1993, in Ronald Weinberger R. and Acker A., eds, Proc. IAU Symp. 155, Planetary nebulae. Kluwer Academic Publishers, Dordrecht, p. 155
Trammell S. R., Goodrich R. W., 1996, ApJ, 468, L107
Treffers R. R., Fink U., Larson H. P., Gautier T. N., III, 1976, ApJ, 209, 793
Webster B. L., Payne P. W., Storey J. W. V., Dopita M. A., 1988, MNRAS, 235, 533
Welch C. A., Frank A., Pipher J. L., Forrest W. J., Woodward C. E., 1999, ApJ, 522, L69

This paper has been typeset from a TEX/ LATEX file prepared by the author.